Microelectronics Reliability 54 (2014) 2133–2137

Contents lists available at ScienceDirect

Microelectronics Reliability

journal homepage: www.elsevier.com/locate/microrel

Electromigration reliability of open TSV structures

W.H. Zisser [a,*], H. Ceric [a,b], J. Weinbub [a], S. Selberherr [a]

[a] Institute for Microelectronics, Technische Universität Wien, Gußhausstraße 27-29/E360, 1040 Wien, Austria
[b] Christian Doppler Laboratory for Reliability Issues in Microelectronics, Austria

ARTICLE INFO

Article history:
Received 26 June 2014
Accepted 14 July 2014
Available online 20 August 2014

Keywords:
Electromigration
Open TSV
Stress simulation

ABSTRACT

Through silicon vias are the components in three-dimensional integrated circuits, which are responsible for the vertical connection inside the dies. In this work we present studies about the reliability of open through silicon vias against electromigration. A two-step approach is followed. In the first step the stress development of a void free structure is analysed by means of simulation to find the locations, where voids due to stress are most probably nucleated. In the second step, voids are placed in the through silicon vias and their evolution is traced including the increase of resistance. The resistance raises more than linearly in time and shows an abrupt open circuit failure. These results are in good agreement with results of time accelerated electromigration tests.

1. Introduction

Three-dimensional (3D) integration is a promising approach for the development of systems with higher performance. Interconnections for 3D integrated circuits, though, include components not used in planar 2D architectures, such as through silicon vias (TSVs). Open TSVs introduced in [1] are a TSV concept in which the cylindrical structure is coated, rather than entirely filled with a conducting metal. Fig. 1 shows the upper part of the TSV including the feeding interconnection. The advantage of this technology is the ability to reduce the stress originating from the mismatched thermal expansion coefficients between the substrate and the TSV.

The reliability of interconnects in integrated circuits is an important issue in microelectronics. Therefore the various degradation processes and their impact on the different components have to be evaluated. One of those processes of particular importance is electromigration (EM), which is essentially the flux of material due to current flow. On the atomistic level EM is the impulse transfer from the conducting electrons to the ionized metal atoms. This degradation process can be divided into two phases. During the first phase the flux of the material leads to the build-up of intrinsic stress. As the stress reaches a certain threshold value, voids can form especially at those locations, where the adhesion of the interconnect metal and the surrounding material is reduced. The formation of a void is the beginning of the second phase. During this second phase, the void grows and migrates, which results in a continuous increase of the interconnect resistance, leading to failure after a certain threshold value is reached. Here we investigate the EM reliability issues of the open TSV technology.

2. Theoretical background

The TSV geometry considered is shown in Fig. 1. The geometrical dimensions given in [1] are used. Here, the tungsten, shown in red, forms an hollow cylinder closed on the bottom side. Below that (not shown in figure because not relevant for the analysis) an aluminium plate is placed on which a solder pump is mounted to connect to other wafers. On the top side, an aluminium layer (shown in blue) forms a second hollow cylinder, which overlaps with the inside, upper part of the tungsten cylinder wall. The upper side of the aluminium connects to the planar interconnect structure by a round plate as shown in Fig. 1. These open TSVs are different compared to the traditional copper TSVs which have their cylinders completely filled.

In order to address EM in materials, two important microscopic forces must be considered to determine the material transport. The first is the so called direct force ($\vec{F}_{direct}$), caused by the local electric field acting on the ionic atoms in the metal. The second is called the wind force ($\vec{F}_{wind}$), which is caused by the electrons scattered by the atoms in the metal [2]. The sum of these two forces determines the total force, as

$$\vec{F} = \vec{F}_{direct} + \vec{F}_{wind} = (Z_d + Z_w)e\vec{E} = Z^* e\vec{E}, \quad (1)$$

* Corresponding author. Tel.: +43 (1) 58801 36031; fax: +43 (1) 58801 936031.
E-mail addresses: zisser@iue.tuwien.ac.at (W.H. Zisser), ceric@iue.tuwien.ac.at (H. Ceric), weinbub@iue.tuwien.ac.at (J. Weinbub), selberherr@iue.tuwien.ac.at (S. Selberherr).

http://dx.doi.org/10.1016/j.microrel.2014.07.099
0026-2714/

where Z_d and Z_w are the so called direct valence and wind valence, respectively, and Z^* is the effective valence, which describes the sensitivity to EM. $\vec{E}$ is the electrical field and e is the elementary electron charge.

For macroscopic modeling of the time evolution of the vacancy distribution C_v in a bulk material, a drift–diffusion model [3] with an additional generation/annihilation term G is used as

$$\frac{\partial C_v}{\partial t} = -\nabla \cdot \vec{J_v} + G. \tag{2}$$

The generation/annihilation term G, usually called Rosenberg-Ohring term [4,5], is computed by

$$G = \frac{C_{v,eq} - C_v}{\tau}, \tag{3}$$

where $C_{v,eq}$ is the equilibrium concentration and τ is the characteristic relaxation time of the vacancy concentration. The vacancy flux $\vec{J}_v$ is driven by three main forces, all of which are included in the bracket of the following equation

$$\vec{J_v} = -D_v\left(\nabla C_v - \frac{|Z^*|}{k_B T} C_v \vec{E} + \frac{f\Omega}{k_B T} C_v \nabla\sigma\right), \tag{4}$$

where k_B is the *Boltzmann* constant, T is the temperature, D_v is the diffusion coefficient of the vacancies, Ω is the atomic volume, f is the relaxation factor, and σ is the hydrostatic stress. The first term in the bracket (first force) is a typical diffusion flux term due to the gradient in the concentrations of vacancies. The second flux term is caused by the EM as described above, which is determined by the electric field in the structure. The third term is the flux due to different stresses in the material. A fourth flux term due to temperature gradients in the material could also be included, but is neglectable in this study, due to the homogenous temperature distribution in the aluminium and the tungsten.

For the stress term a solid mechanics simulation is required. The inelastic strain ϵ^v due to vacancy pileup and creation/annihilation, which serves as an input to the solid mechanics simulation, is obtained by the following equation [6].

$$\frac{\partial \epsilon^v}{\partial t} = \Omega[(1-f)\nabla \cdot \vec{J_v} + fG] \tag{5}$$

The geometry considered in our calculations is a segment of an open TSV, cf. Fig. 2. The tungsten, (green), forms an arc. On the topside, an aluminium layer (yellow) forms a second arc, which overlaps with the inside upper part of the tungsten arc wall. The upper side of the aluminium connects to the adjacent planar aluminium interconnect. In the inner part of the TSV the aluminium and the tungsten arc are coated by a silicon oxide film (red).

The blue line indicates a reference for subsequent simulations introduced in Section 3.

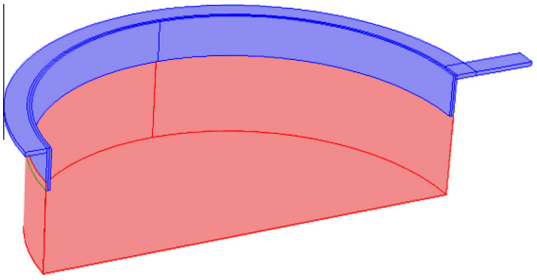

Fig. 1. TSV structure: aluminium in blue and tungsten in red. The tungsten cylinder is shortened to 10% of the real length. For the simulated TSV the upper plate is removed. (For interpretation of the references to colour in this figure legend, the reader is referred to the web version of this article.)

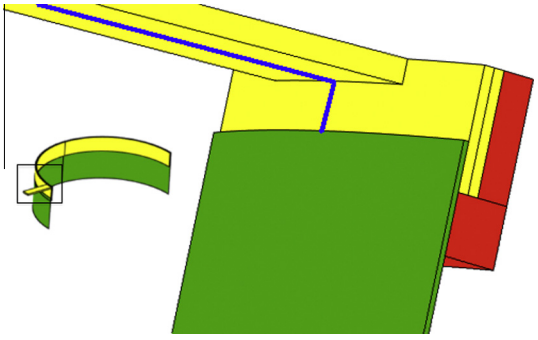

Fig. 2. Total and zoomed-in detail view of the TSV structure with aluminium in yellow, tungsten in green, and silicon oxide in red. The blue line is a reference for the cut and the mirrored boundary condition applied in Section 3. (For interpretation of the references to colour in this figure legend, the reader is referred to the web version of this article.)

Since previous studies have shown that tungsten has a much lower sensitivity to EM [7], the flux of material is considered only in the aluminium part of the TSV. The aluminium and tungsten layers are mechanically fixed to the silicon oxide. The mechanical constraints for the outer surface of the material is considered to be fixed and the inner surface of the silicon oxide layer is free to move, as in the actual structure.

In the case the void nucleation condition is reached, a void is placed. The physics of the void evolution is described by the phase field model which comprises material transport at the void surface induced by EM and mechanical stress [8]. Thereby an order parameter ϕ is defined, which determines the areas where metal is ($\phi = 1$) and is not ($\phi = -1$) located and forms a void. The development of the order parameter in time is described by the differential equation

$$\frac{\partial \phi}{\partial t} = \frac{2}{\epsilon_{pf}\pi}\nabla \cdot \mathcal{D}_s(\phi)\left(\nabla\mu_s - eZ\vec{E}\right) - \frac{4A}{\epsilon_{pf}\pi}(\mu_s - \mu_v). \tag{6}$$

μ_s and μ_v represent the chemical potentials of the surface and the vacancies in bulk, respectively, A is a rate parameter, $\mathcal{D}_s$ is the surface diffusion, and the second term of the first summand ($eZ\vec{E}$) represents the EM. As the order parameter is a continues function, the values between the metal and the void values are between $+1$ and -1. Only in these sectors the second term is contributing to the equation. The thickness of the interface region can be adjusted by ϵ_{pf}. The lower limit for this parameter is bounded by the mesh resolution to ensure an appropriate number of elements inside the diffuse interface region for a smooth transition of the order parameter ϕ. The minimum curvature of the interface yields the upper limit for ϵ_{pf}.

3. Results

Using the above mentioned models numerical simulations with the finite element method have been carried out.

Fig. 3 shows the current distribution in the open TSV segment and the arrow indicates the current direction. The current densities in the two metals differ strongly due to the different thicknesses of the metal layers. Furthermore, in the regions where the aluminium is overlapped by the tungsten the current is mainly flowing in the aluminium due to its lower resistance.

Fig. 4 shows the development of the maximum relative concentration change of vacancies in time. Three phases can be clearly distinguished. In the first phase EM dominates the transport of vacancies which accumulate close to the tungsten/aluminium interface. The response of the metal represented by the stress gra-

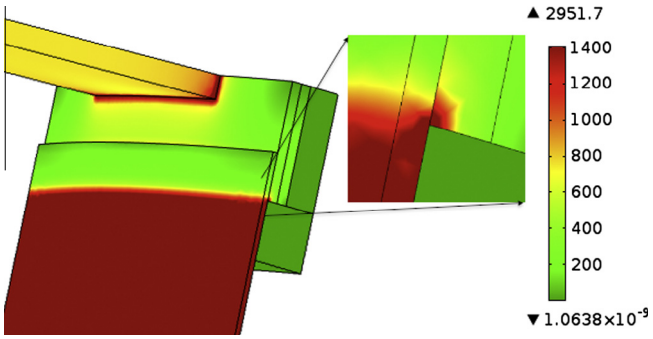

Fig. 3. Current density in the structure (A/cm^2). The arrow shows the direction of the current flow. The inset is a zoom-in at the corner of the aluminium/tungsten interface to show the maximum current density in the overlapping area.

dient and vacancy concentration gradient is in this phase significantly smaller than the EM.

After a certain time (~ 1 s) the concentration reaches a quasi-steady state due to the compensation of the EM flux by the stress gradient induced flux and the concentration gradient induced flux, which tend to oppose EM. This phase is followed by an abrupt rise of the vacancy concentration (> 10 ks), which is caused by stress activated vacancy sources, e.g., grain boundaries. This phenomenon was already studied by Kirchheim [9].

Fig. 5 shows the stress development in time during the three phases of the vacancy dynamics. During the third phase of the vacancy pileup of EM, the stress reaches a threshold for void nucleation.

The stress distribution in the structure identifies the location with the highest probability for void nucleation and is shown in Fig. 6. The highest stress is observed in the interface regions of the aluminium, because the EM induced shrinking leads to different strains.

In order to investigate the dynamics of void evolution, an initial void is placed at the site, which shows the highest stress level. In this structure the void was placed on the aluminium/tungsten interface at the blue line depicted in Fig. 2 above the end of the aluminium part. This is the starting condition of the second step of the simulation, where the resistance increase due to the growth of the void is investigated.

Fig. 7 shows the position of the initial void placed for the resistance development calculation. There the order parameter in the aluminium is shown. The blue region represents the void with a order parameter $\phi = -1$ and the red region with $\phi = 1$. Due to the mirror symmetry of the structure and of the placed void only half of the structure was simulated with the mirror boundary condition applied to the blue cutting line shown in Fig. 2. After some time the void moves in current direction to the end of the aluminium and reforms into a half circle due to energy minimisation leading to surface minimisation (Fig. 8). This process is followed by the

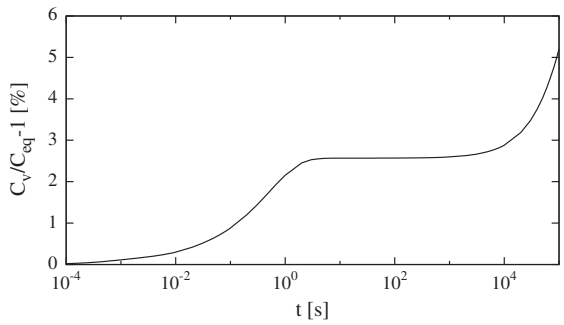

Fig. 4. Maximum relative concentration change of vacancies over time in the open TSV without a void nucleated.

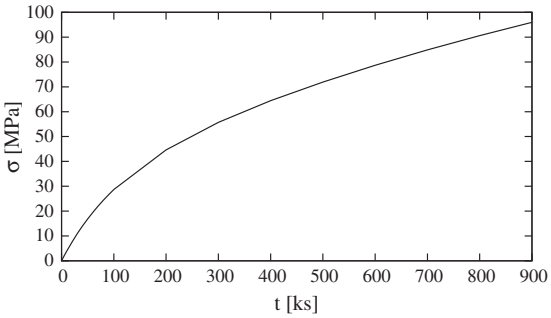

Fig. 5. Maximum stress versus time in the open TSV without a void nucleated.

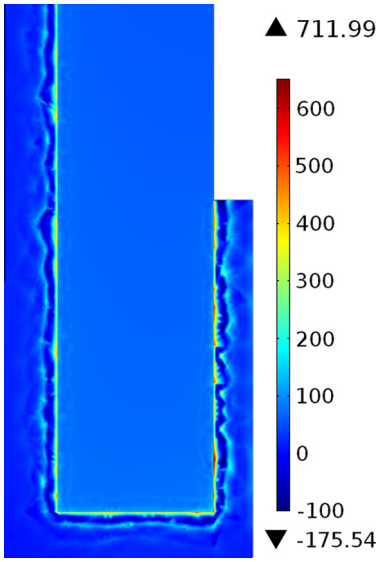

Fig. 6. Stress (in MPa) in the plane shown in blue in Fig. 2 after 1Ms of current flow. The peak values are located in the interface regions. (For interpretation of the references to colour in this figure legend, the reader is referred to the web version of this article.)

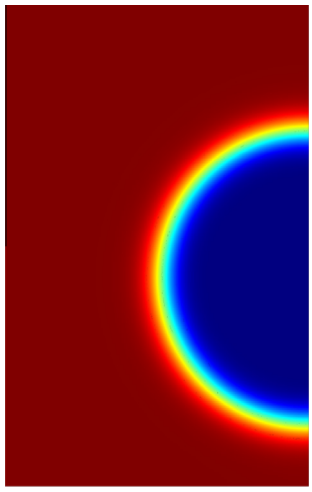

Fig. 7. Order parameter distribution (ϕ) of the initial void placed in the structure. Only the cylindrical aluminium section is shown. A mirror boundary condition is applied to the right side, which represents the blue line of Fig. 2. Red represents the metal ($\phi = 1$) and blue the void ($\phi = -1$). (For interpretation of the references to colour in this figure legend, the reader is referred to the web version of this article.)

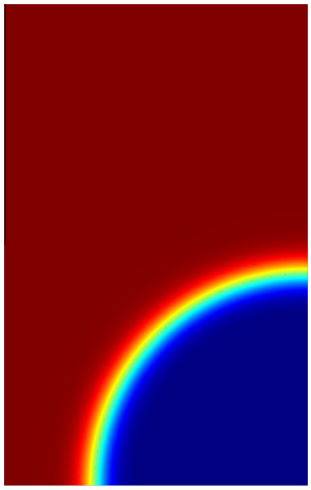

Fig. 8. Order parameter distribution (ϕ) of the void that has migrated to the end of the aluminium. Only the aluminium section is shown. The right edge is located at the blue line of Fig. 2. Red represents the metal ($\phi = 1$) and blue the void ($\phi = -1$). (For interpretation of the references to colour in this figure legend, the reader is referred to the web version of this article.)

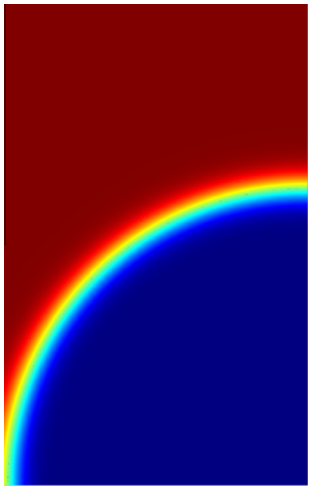

Fig. 9. Order parameter distribution (ϕ) after the void has migrated to the end of the aluminium. The started growth process continues, until the failure criterion is reached. Only the aluminium section is shown. The right edge is located at the blue line of Fig. 2. Red represents the metal ($\phi = 1$) and blue the void ($\phi = -1$). (For interpretation of the references to colour in this figure legend, the reader is referred to the web version of this article.)

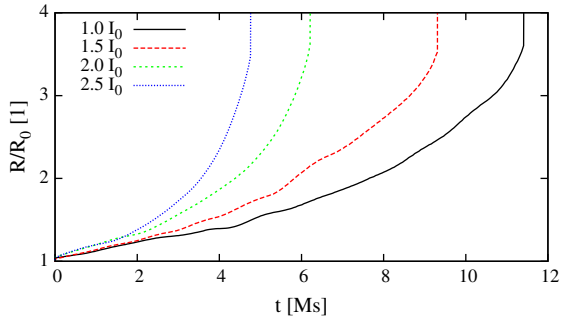

Fig. 10. Relative resistance of the TSV versus time with a growing void for different current densities.

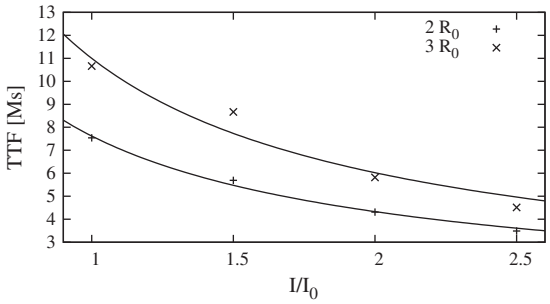

Fig. 11. TTF for different current densities. Failure criteria: two and three times of the initial resistance. Lines indicate the fitting according to Blacks's equation.

void growing, which in turn leads to increased resistance shown in Fig. 9.

In Fig. 10 the resistance development over time of the interconnect structure for different current densities is shown. With the growth of the void, the current density at the void surface also increases as the conducting cross-section is decreasing and leads to higher EM flux, resulting in a nonlinear resistance increase. At the end an abrupt resistance increase (for the $2.5I_0$ case at 4.7Ms) leading to an open circuit failure can be observed. This observations are consistent with the resistance change measured in accelerated EM tests for dual damascene structures [10] and filled TSV structures [11].

The increased resistance of the interconnect triggers circuit failure due to an altered electrical behaviour. Fig. 11 shows for two different failure criteria the time to failure (TTF). The first threshold criterion was chosen to be the doubled (+) and the second the tripled ($\times$) initial resistance. The fitting to Black's equation shows an exponent of -0.81 for the double resistance criterion and for the triple resistance criterion of -0.86 in good accordance with the experimentally observed values [12].

4. Summary

In this work we describe a two-step approach to analyze EM in open TSV technology by means of simulation employing the finite element method.

First the locations with the highest probability of nucleating a void are identified in a void free structure. Then a void is introduced in the highest stress site and is allowed to evolve in time. As a constant current through the structure is used a more than linear growth in resistance with an open circuit failure is observed.

Acknowledgment

This work was supported by the Austrian Science Fund FWF, Project P23296-N13.

References

[1] Kraft J, Schrank F, Teva J, Siegert J, Koppitsch G, Cassidy C, et al. 3D sensor application with open through silicon via technology. Proc ECTC 2011:560–6.
[2] Sorbello RS. Microscopic driving forces for electromigration. Proc Mater Res Soc Symp 1996;427:73–81.
[3] de Orio R, Ceric H, Selberherr S. A compact model for early electromigration failures of copper dual-damascene interconnects. Microelectron Reliab 2011;51(9–11):1573–7.
[4] Rosenberg R, Ohring M. Void formation and growth during electromigration in thin films. J Appl Phys 1971;42(13):5671–9.
[5] Ceric H, de Orio RL, Cervenka J, Selberherr S. A comprehensive TCAD approach for assessing electromigration reliability of modern interconnects. IEEE Trans Device Mater Reliab 2009;9(1):9–19.
[6] Ceric H, Heinzl R, Hollauer C, Grasser T, Selberherr S. Microstructure and stress aspects of electromigration modeling. Proc AIP 2006;817(1):262–8.

[7] Tao J, Young K, Cheung NW, Hu C. Electromigration reliability of tungsten and aluminum vias and improvements under AC current stress. IEEE Trans Electron Dev 1993;40(8):1398–405.
[8] Bhate DN, Kumar A, Bower AF. Diffuse interface model for electromigration and stress voiding. J Appl Phys 2000;87(4):1712–21.
[9] Kirchheim R. Stress and electromigration in Al-lines of integrated circuits. ACTA Metall Mater 1992;40(2):309–23.
[10] M. Hauschildt, Statistical analysis of electromigration lifetimes and void evolution in Cu interconnects, Ph.D. Thesis, University of Texas in Austin, USA; 2005.
[11] Moreau S, Bouchu D. Reliability of dual damascene TSV for high density integration: The electromigration issue. Proc IRPS 2013:CP.1.1–5.
[12] Oates A, Lin M. Electromigration failure distributions of Cu/low-k dual-damascene vias: impact of the critical current density and a new reliability extrapolation methodology. IEEE Trans Device Mater Reliab 2009;9(2):244–54.